

# Fluid/solid coupled heat transfer analysis of a free rotating disc

PAVEL V. BULAT<sup>a\*</sup>  
KONSTANTIN N. VOLKOV<sup>b</sup>

<sup>a</sup> ITMO University, St Petersburg, 197101, Russia

<sup>b</sup> Kingston University, London, SW15 3DW, United Kingdom

**Abstract** The coupled fluid/solid heat transfer computations are performed to predict the temperatures reached in the rotating disc systems. An efficient finite element analysis (FEA) and computational fluid dynamics (CFD) thermal coupling technique is developed and demonstrated. The thermal coupling is achieved by an iterative procedure between FEA and CFD calculations. In the coupling procedure, FEA simulation is treated as unsteady for a given transient cycle. To speed up the thermal coupling, steady CFD calculations are employed, considering that fluid flow time scales are much shorter than those for the solid heat conduction and therefore the influence of unsteadiness in fluid regions is negligible. To facilitate the thermal coupling, the procedure is designed to allow a set of CFD models to be defined at key time points/intervals in the transient cycle and to be invoked during the coupling process at specified time points. The computational procedure is applied to predict heat transfer characteristics of a free rotating disc.

**Keywords:** Heat transfer; Coupled analysis; Computational fluid dynamics; Finite element analysis; Disc; Rotating cavity

## 1 Introduction

An accurate prediction of metal temperatures is an important problem in the gas turbine design and optimization. The coupled fluid/solid heat

---

\*Corresponding Author. Email: bulat.itmo@bk.ru

transfer computations are widely used to predict the temperatures reached in the rotor/stator disc cavities. Development and improvement of the prediction methods and tools helps to automate aerothermal analysis and to reduce gas turbine design and testing costs [1].

To assist gas turbine design, accurate and fast prediction of component metal temperature is one of the key issues. In industry, finite element analysis (FEA) is routinely used to predict metal temperatures with the thermal boundary conditions provided by thermocouple measurements and empirical correlations. The limitation of this practice is obvious. Its effectiveness is subject to availability and applicability of the current database and correlations for a new design.

With rapid progress of computational fluid dynamics (CFD) and computer power, CFD has proven to be a useful tool to assist and to improve the metal temperature predictions [2]. There are three types of approaches in using CFD solutions for fluid/solid heat transfer calculations. One is generally referred to as conjugate heat transfer analysis, the second is referred to as non-coupled FEA/CFD procedure, and the third one referred to as coupled FEA/CFD analysis.

In conjugate analysis, the fluid/solid heat transfer calculations are realized by expanding the CFD capability to include heat conduction calculations in solid regions neighbouring the fluids [3,4]. A number of studies have been performed showing application of the conjugate analysis for engine component temperature predictions, such as a real turbine rotor/stator system simulation [5], a blade film cooling prediction [6], and an internally cooled turbine blade application [7]. It was found that the applications of the conjugate analysis were limited to steady and simple transient calculations. A CFD simulation is expensive, and this would be especially true for a time accurate calculation of a flight cycle, as a relatively small time step has to be used to resolve the flow unsteadiness. Therefore, the computational cost of performing a transient conjugate flight cycle analysis with an unsteady CFD solution is prohibitive.

Non-coupled procedures reduces the CFD cost, where only a limited number of steady CFD calculations are performed at key engine operating conditions to produce a set of CFD-based correlations, which provide the necessary thermal boundary conditions for FEA calculations. Typical examples include turbine disc cavity applications considered in [8,9]. However, successful application of the non-coupled procedure is dependent on user experience and expertise, such as boundary segment partitioning for

the discrete correlations. The use of discrete correlations over a continuous wall could also be a concern for potential degradation of thermal solution accuracy.

Coupled FEA/CFD analysis is an alternative technique, where separate FEA and CFD codes are used for solid and fluid regions with a smooth exchange of information between the two codes to ensure continuity of temperature and heat flux. There are a variety of approaches in implementing the coupled FEA/CFD analysis. For instance, 3D FEA to 3D CFD coupling procedure is demonstrated in [10] for cooled turbine blade application. A coupled finite volume method and boundary element method approach with application to turbine blade calculation is described in [11]. Coupled procedure for film-cooled turbine blade applications is reported in [12]. An efficient coupling procedure of in-house FEA code to a commercial CFD code is reported in [13]. This procedure is successfully applied to turbine disc cavity calculations for flight cycle simulations and steady state coupling in [14,15].

To further enhance computational efficiency, a frozen flow or energy equation only coupling option is also developed in [13, 15], where just energy equation is solved while the flow is frozen in CFD simulation during the thermal coupling process for specified time intervals. This option has proven very useful in practice, as the flow is found to be unaffected by the thermal boundary conditions over certain time intervals.

In this study, the coupled heat transfer calculations are performed based on full coupling procedure between FEA and CFD code and simplified coupling procedure based on energy equation option. To speed up the thermal coupling, steady CFD calculations are employed, considering that fluid flow timescales are much shorter than those for the solid heat conduction and therefore the influence of unsteadiness in fluid regions is negligible. To facilitate the thermal coupling, the procedure is designed to allow a set of CFD models to be defined at key time points/intervals in the transient cycle and to be invoked during the coupling process at specified time points. Multi-grid and Krylov subspace methods are applied to solve energy conservation equation in the fluid domain and their efficiencies are compared.

## 2 Methodology

The mathematical model includes equations describing temperature distribution in the solid domain and equations describing distributions of pres-

sure, velocity and temperature in the fluid domain.

## 2.1 Solid domain

The thermal analysis consists in calculation of the temperature distribution and the thermal parameters of the system. It is based on the heat balance equation obtained in accordance with the energy conservation law, for whose discretization the finite element method is used. In addition to the calculation of the temperature field, the heat flux at the boundary of the system and the heat transfer coefficients are found as a result of the thermal analysis for the given temperature of surrounding fluid [16].

In the Cartesian frame of reference  $(x, y, z)$ , the energy conservation equation has the form

$$\rho c \frac{\partial T}{\partial t} = \frac{\partial}{\partial x} \left( \lambda \frac{\partial T}{\partial x} \right) + \frac{\partial}{\partial y} \left( \lambda \frac{\partial T}{\partial y} \right) + \frac{\partial}{\partial z} \left( \lambda \frac{\partial T}{\partial z} \right), \quad (1)$$

where  $t$  is the time,  $x$ ,  $y$ , and  $z$  are the Cartesian coordinates,  $\rho$  is density,  $c$  is the specific heat capacity,  $\lambda$  is the thermal conductivity, and  $T$  is the temperature. The internal heat sources in Eq. (1) are neglected.

Titanium is used as a material of rotating wall, and steel is used as a material of stationary wall. The thermophysical properties of material are functions of temperature.

## 2.2 Fluid domain

The turbulent flow of viscous compressible gas is described with the Reynolds-averaged Navier-Stokes (RANS) equations and the equations of the modified  $k-\varepsilon$  turbulence model, for whose discretization finite volume method is used. As a result of the integration of flow equations, the velocity, pressure and temperature distributions in fluid domain are found.

In Cartesian frame of reference the governing equation takes the form

$$\frac{\partial Q}{\partial t} + \frac{\partial F_x}{\partial x} + \frac{\partial F_y}{\partial y} + \frac{\partial F_z}{\partial z} = H, \quad (2)$$

where  $Q$  is the vector of conservative variables,  $F_x$ ,  $F_y$ , and  $F_z$  are the vectors of inviscid and viscous fluxes, and  $H$  is the source term. The system of Eq. (2) includes the mass conservation equation (continuity equation), momentum conservation equation and energy conservation equation. The conservation equations written in the form (2) are applicable to absolute and relative velocity formulations.

To complete the system of Eqs. (2), pressure of an ideal gas is calculated as

$$p = (\gamma - 1)\rho(e - q^2/2), \quad (3)$$

where  $\gamma$  is the ratio of specific heat capacities at constant pressure and constant volume,  $p$  in the pressure,  $e$  is the specific total energy. The velocity magnitude is

$$q^2 = (v_x^2 + v_y^2 + v_z^2) - \omega^2 r^2,$$

where  $r$  is the rotation radius,  $\omega$  is the rotation speed.

The vector of conservative variables and the flux vectors have the following form:

$$Q = \begin{pmatrix} \rho \\ \rho v_x \\ \rho v_y \\ \rho v_z \\ \rho e \end{pmatrix},$$

$$F_x = \begin{pmatrix} \rho v_x \\ \rho v_x v_x + p - \tau_{xx} \\ \rho v_x v_y - \tau_{xy} \\ \rho v_x v_z - \tau_{xz} \\ (\rho e + p)v_x - v_x \tau_{xx} - v_y \tau_{xy} - v_z \tau_{xz} + q_x \end{pmatrix},$$

$$F_y = \begin{pmatrix} \rho v_y \\ \rho v_y v_x - \tau_{yx} \\ \rho v_y v_y + p - \tau_{yy} \\ \rho v_y v_z - \tau_{yz} \\ (\rho e + p)v_y - v_x \tau_{yx} - v_y \tau_{yy} - v_z \tau_{yz} + q_y \end{pmatrix},$$

$$F_z = \begin{pmatrix} \rho v_z \\ \rho v_z v_x - \tau_{zx} \\ \rho v_z v_y - \tau_{zy} \\ \rho v_z v_z + p - \tau_{zz} \\ (\rho e + p)v_z - v_x \tau_{zx} - v_y \tau_{zy} - v_z \tau_{zz} + q_z \end{pmatrix}.$$

Here,  $t$  is the time,  $x$ ,  $y$ , and  $z$  are the Cartesian coordinates,  $\rho$  is density,  $v_x$ ,  $v_y$  and  $v_z$  are the Cartesian velocity components. To model flows that include rotating boundaries, the rotating frame of reference is used. The flow may be unsteady in an inertial frame (a domain fixed in the laboratory frame), but steady relative to the rotating non-inertial frame (the

domain moving with the rotating part). The non-inertial character of the reference system is taken into account by introducing the Coriolis force and centrifugal force in the source term

$$H = \begin{pmatrix} 0 \\ 0 \\ \rho\omega(y\omega + 2v_z) \\ \rho\omega(z\omega - 2v_y) \\ 0 \end{pmatrix}.$$

The viscous stress tensor is defined as

$$\tau_{ij} = \mu_e \left( \frac{\partial v_i}{\partial x_j} + \frac{\partial v_j}{\partial x_i} - \frac{2}{3} \frac{\partial v_k}{\partial x_k} \delta_{ij} \right).$$

The heat flux is given by Fourier law

$$q_i = -\lambda_e \frac{\partial T}{\partial x_i}$$

where  $T$  is the temperature. The effective viscosity is calculated as a sum of the molecular and turbulent viscosities

$$\mu_e = \mu + \mu_t,$$

The molecular viscosity,  $\mu$ , is a function of temperature. It is modelled by Sutherland's law

$$\frac{\mu}{\mu_*} = \left( \frac{T}{T_*} \right)^{3/2} \frac{T_* + S_0}{T + S_0},$$

where  $\mu_*$  and  $T_*$  are reference viscosity and temperature, and  $S_0$  is a constant determined experimentally, so that  $\mu_* = 1.68 \times 10^{-5}$  kg/(ms),  $T_* = 273$  K, and  $S_0 = 110.5$  K for air. The thermal conductivity is linked to the specific heat capacity at constant pressure,  $C_p$ , and the Prandtl number,  $\text{Pr}$ , so that  $\lambda = c_p \mu / \text{Pr}$  and  $\text{Pr} = 0.7$  for air.

The turbulent viscosity is calculated by the Kolmogorov-Prandtl formula

$$\mu_t = c_\mu \rho \frac{k^2}{\varepsilon},$$

where  $k$  is the turbulent kinetic energy, and  $\varepsilon$  is the dissipation rate. The effective thermal conductivity is expressed in terms of the viscosity and the Prandtl number

$$\lambda_e = c_p \left( \frac{\mu}{\text{Pr}} + \frac{\mu_t}{\text{Pr}_t} \right).$$

The turbulent thermal conductivity is calculated using turbulent Prandtl number, which is  $\text{Pr}_t = 0.9$  for air.

### 2.3 Turbulence model

The  $k$ - $\varepsilon$  model of Launder and Spalding [17] is used to close RANS equations written in the form (1). The  $k$ - $\varepsilon$  turbulence model solves two transport equations for the turbulent kinetic energy and its dissipation rate [17]. The transport equation for the turbulent kinetic energy is derived from the exact equation, while the transport equation for its dissipation rate is obtained using physical reasoning and has a little resemblance to its mathematically exact counterpart.

The transport equations of  $k$ - $\varepsilon$  turbulence model are written in the following form [17]:

$$\frac{\partial \rho k}{\partial t} + (\rho \mathbf{v} \cdot \nabla) k = \nabla \cdot \left[ \left( \mu + \frac{\mu_t}{\sigma_k} \right) \nabla k \right] + P - \rho \varepsilon, \quad (4)$$

$$\frac{\partial \rho \varepsilon}{\partial t} + (\rho \mathbf{v} \cdot \nabla) \varepsilon = \nabla \cdot \left[ \left( \mu + \frac{\mu_t}{\sigma_\varepsilon} \right) \nabla \varepsilon \right] + \frac{\varepsilon}{k} (c_{\varepsilon 1} P - c_{\varepsilon 2} \rho \varepsilon). \quad (5)$$

The turbulence production term, resulting from interaction between the mean flow and the turbulence field, is

$$P = \left( 2\mu_t S_{ij} - \frac{2}{3}\rho k \delta_{ij} \right) \frac{\partial v_i}{\partial x_j}.$$

The components of the strain rate tensor are

$$S_{ij} = \frac{1}{2} \left( \frac{\partial v_i}{\partial x_j} + \frac{\partial v_j}{\partial x_i} \right).$$

The coefficients of  $k$ - $\varepsilon$  model have the following default values  $c_\mu = 0.09$ ,  $\sigma_k = 1.0$ ,  $\sigma_\varepsilon = 1.3$ ,  $c_{\varepsilon 1} = 1.44$ ,  $c_{\varepsilon 2} = 1.92$ .

In a stagnation flow, high level of strain rate produces excessive levels of turbulent kinetic energy whereas deformation near stagnation point is nearly irrotational. To prevent the generation of non-physical levels of turbulent viscosity in strained but irrotational flow, the Kato-Launder correction to production term is used [18]. The production term in equation (4) is modified as follows:

$$P = \mu_t \left( 2S_{ij} \frac{\partial v_i}{\partial x_j} \right)^{3/2} (\Omega_{ij} \Omega_{ij})^{1/2}. \quad (6)$$

The components of rotation tensor are

$$\Omega_{ij} = \frac{1}{2} \left( \frac{\partial v_i}{\partial x_j} - \frac{\partial v_j}{\partial x_i} \right).$$

This correction of production term leads to a marked reduction in energy production near the stagnation point, while having no effect in a simple shear flow.

A hybrid form of the production term is proposed in [19], in which the standard form of production term and Kato-Launder correction are averaged

$$P = \mu_t |S| [(1-\alpha) |S| + \alpha |\Omega|],$$

where  $0 < \alpha < 1$  is a weighting factor. The invariants of strain rate tensor and rotation tensor are

$$|S| = (2S_{ij}S_{ij})^{1/2}, \quad |\Omega| = (2\Omega_{ij}\Omega_{ij})^{1/2}.$$

The hybrid model is particularly used for stagnation flows. In that case the weighting factor is chosen to be  $\alpha = 0.85$ , as recommended in [19].

To account for rotational effects and curvature of stream lines in the transport equations of the  $k$ - $\varepsilon$  model, the method proposed in [20] and generalized in [21,22] is used. The eddy viscosity is obtained from the equation

$$\mu_t = c_\mu f_c \rho \frac{k^2}{\varepsilon},$$

where  $c_\mu$  is the usual model constant ( $c_\mu = 0.09$ ), and  $f_c$  is a damping function given by [20]

$$f_c = \frac{1}{1 + c_c \text{Ri}_t}.$$

An additional model constant is  $c_c = 0.1$ . The restriction  $0.02 < c_c c_\mu < 0.15$  is also employed. The turbulent Richardson number,  $\text{Ri}_t$ , is defined as [21,22]

$$\text{Ri}_t = \frac{q}{R_c} (\mathbf{b} \cdot \boldsymbol{\Omega}) \left( \frac{\varepsilon}{k} \right)^{-2},$$

where  $q$  is the velocity magnitude,  $\boldsymbol{\Omega}$  is the vorticity,  $R_c$  is the local radius of curvature of stream line, and  $\mathbf{b}$  is the unit vector of bi-normal to the stream line.

## 2.4 Coupling procedure

Coupled thermal analysis is normally run transiently. Cycle parameters are defined at discrete time points (ramp points) throughout the time span of the transient, to form the cycle definition. If a value of a cycle parameter changes from one ramp point to the next, the parameter is linearly interpolated with respect to time between those two ramp points. An example of a cycle definition for rotation speed is shown in Fig. 1 (nodal points correspond to different time moments when rotation speed changes).

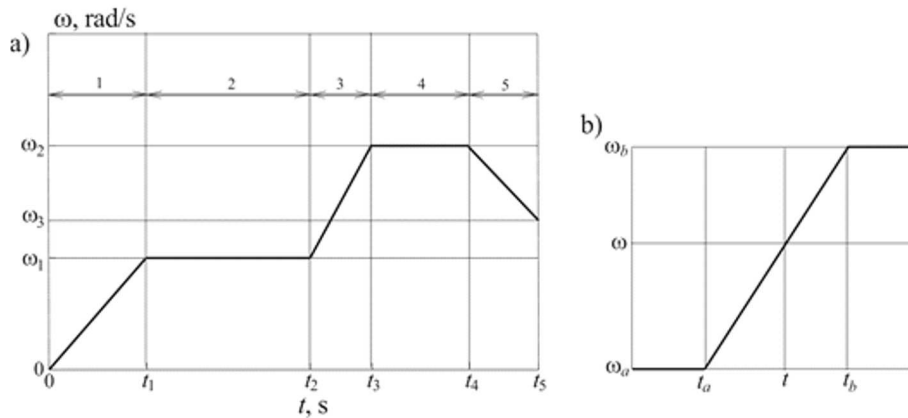


Figure 1: Cycle definition (a) and linear interpolation of cycle parameter (b).

In the engine cycle models, the FEA calculations are unsteady to reproduce the relatively slow response of metal heat conduction to a change in operating conditions over a given transient flight cycle. Compared to this, the fluid flow timescales are much shorter, as they are determined by the fast convection of the flow. As a result, the influence of unsteadiness of fluid flow is expected to be negligible, and steady CFD calculations may be employed. In other words, the flow is assumed to adjust instantaneously to changes in the flow boundary conditions, as the time taken for such adjustments is much smaller than other time scales for the problem considered. This saves considerable computing time for a FEA/CFD thermal coupling computations, as it avoids expensive unsteady CFD simulation in fluid regions and allows much larger time steps for unsteady FEA simulation of the metal heat conduction in solid regions, which means fewer time steps are needed to resolve a given transient cycle. Further approximation is usually involved in modelling engine accelerations or decelerations when

the rotation speed is changing.

The coupling is realized through an iterative loop between the FEA and CFD simulations using under relaxation procedure, with communications ensuring continuity of temperature and heat flux across the coupled boundaries between the FEA and CFD models. Convergence of the thermal coupling at a thermal time point is recognized when the difference of coupled wall temperature between two adjacent successive thermal coupling iterations is reduced to a required tolerance. In the coupling process, intermediate individual FEA and CFD solutions are obtained in turn with dynamically updated boundary conditions. On coupling walls, the temperature distributions obtained in FEA simulations are used to define temperature boundary conditions for CFD models, and the heat flux distributions obtained in CFD simulations are used to define heat flux boundary conditions for the FEA model. Convergence of the individual FEA and CFD solutions is recognized when their governing equations residuals are reduced to a required tolerance. To avoid exceptional dead lock of the individual CFD simulations, appropriate maximum numbers of iterations are assigned for each CFD model. The practice is implemented in a similar way to that for ordinary isolated CFD calculations.

### 3 Numerical method

To simulate the fluid flow and calculate the thermal loads in a system, the FEA solver is used for calculation of temperature field in a solid domain and the CFD solver is used for calculation of fluid flowfield. The communication procedure is employed in order to exchange boundary values between FEA model and CFD model.

To discretize the Eq. (1), the finite element method and the implicit time scheme described in [23] are used. In order to solve the system of algebraic equations, different iterative methods are used. Newton-Raphson method is applied to solve the system of algebraic equations. To simplify its realization, the derivatives of thermophysical parameters with respect to the temperature are neglected in calculation of the Jacobian. As the initial approximation of the solution, linear extrapolation of the temperature from the previous time step is used. Iterations terminate if the residual does not exceed the given accuracy (in the calculations  $10^{-3}$ ). To update the solution, the lower relaxation procedure with relaxation factor of 0.5 is used.

The numerical calculations of fluid flow are based on an unstructured hybrid code, using the finite volume method and an edge-based data structure to give the flexibility to run on meshes composed of a variety of cell types. This has the advantage that hexahedral or prismatic elements can be used to capture velocity gradients through the boundary layer adjacent to a surface. At the same time, hybrid meshes can incorporate pyramid and tetrahedral cells in the free stream regions to provide greater flexibility to represent complex geometries.

The non-linear solver works in an explicit time-marching technique, based on a five-step Runge-Kutta stepping procedure. Convergence to a steady state is accelerated by the use of multigrid techniques, and by the application of block-Jacobi preconditioning for high-speed flows, together with a separate low Mach number preconditioning method for use with low-speed flows. The sequence of meshes is created using an edge-collapsing algorithm. Preconditioning improves the rate at which information propagates through the flow domain during the solution iterations.

Convergence acceleration becomes the key issue for enabling practical use of higher-order discretizations of the fluid flow equations on unstructured meshes. Multigrid and GMRES (generalized minimal residual) methods are used to solve energy conservation equation in the fluid domain [24]. The GMRES method is an iterative method for the numerical solution of a system of linear equations. The method approximates the solution by the vector in a Krylov subspace with a minimal residual. The Arnoldi iteration uses the stabilized Gram-Schmidt process to produce a sequence of orthonormal vectors. Arnoldi method reduces a dense matrix into Hessenberg form. The eigenvalues of the Hessenberg matrix are obtained from a number of steps smaller than could provide accurate approximations to some eigenvalues of the original matrix. Modified Gram-Schmidt (MGS) procedure is used to find orthonormal basis at each step of Arnoldi iteration.

## 4 Results

A disc rotating in a viscous fluid is the simplest configuration for which rotating must be taken into account.

### 4.1 Model

A system consisting of a rotating disc having 24 holes spaced at regular intervals and a shaft is considered. The solid components are represented

in a 2D axisymmetric solid model, and the fluid domain is treated as 2D axisymmetric model or 3D model with periodic boundary conditions in circumferential direction.

In the calculations, an axisymmetric model, presented in Fig. 2a, or 3D sector model (15 degrees), shown in Fig. 2b, are used. The inner and outer radii of the shaft are  $a_1 = 0.1$  m and  $a_2 = 0.12$  m, and the inner and outer radii of the disc are  $b_1 = 0.14$  m and  $b_2 = 0.3$  m, respectively. The radius of the hole and the radial coordinate of its centre are  $d_1 = 0.01$  m and  $d_2 = 0.26$  m, and the thickness of the disc and the length of the computational domain are  $s = 0.03$  m and  $l = 0.23$  m, respectively.

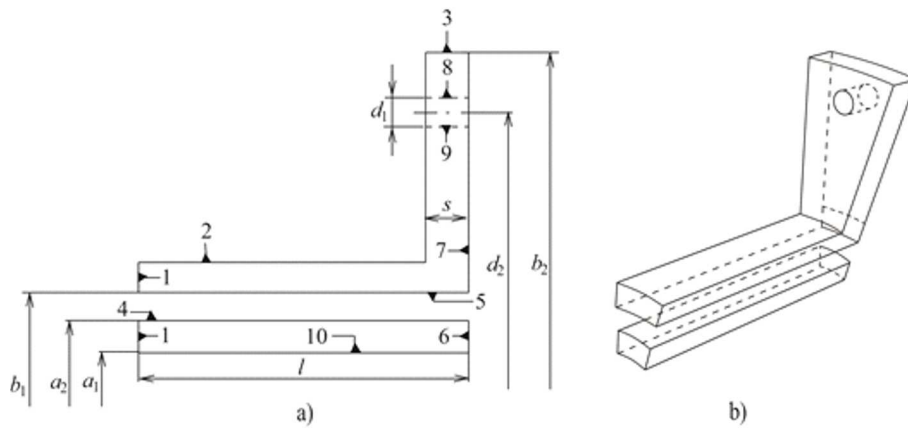


Figure 2: 2D model (a) and 3D model (b).

The 3D regions occupied by the fluid are shown in Fig. 3. Region I, presented in Fig. 3a, takes into account the fluid flow in the gap between the rotor and the shaft, and region II, presented in Fig. 3b, takes into account the influence of the external flow on the heat transfer of the rotating disc and the flow in the hole. The location of control points on the disc and the shaft at which the temperature is measured is shown in Fig. 4.

## 4.2 Cycle definition

The loading cycles used for the 2D or 3D thermal simulations and coupled calculations are shown in Fig. 5. The cycle parameters are the rotation speed of the disc (line 1) and the rotation speed of the shaft (line 2).

For thermal simulation, the length of the cycle is 3000 s, as shown in Fig. 5a, including two regions of the rotation acceleration of the disc and the shaft

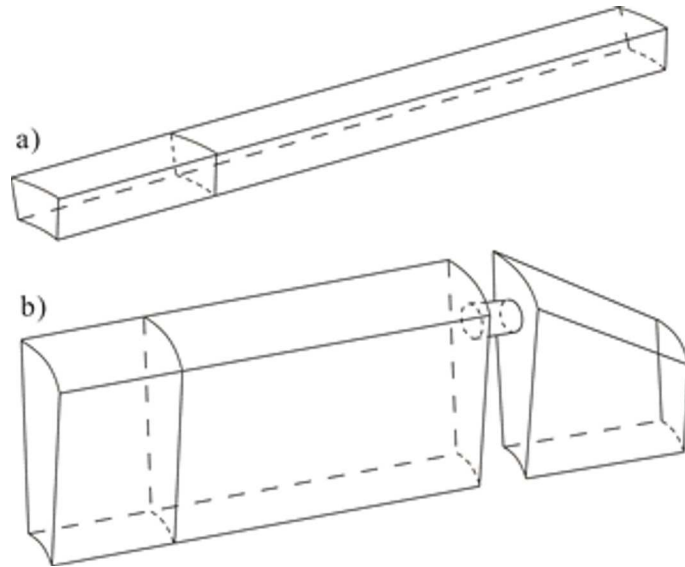


Figure 3: CFD models in region I (a) and region II (b).

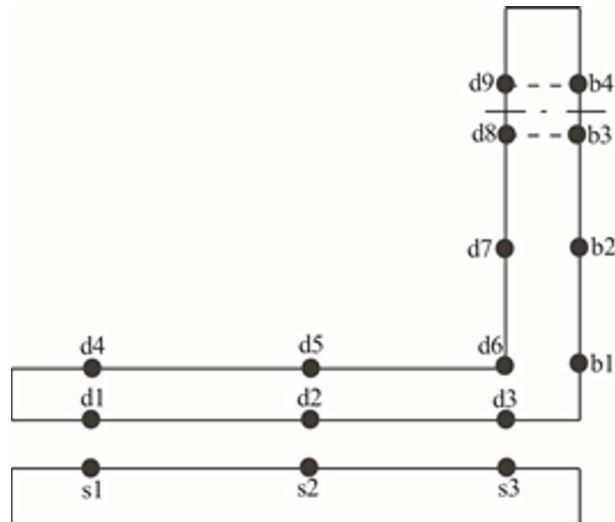


Figure 4: Location of control points.

(regions between ramp points 1 and 2, 3 and 4), the rotation slowing down region (region between ramp points 5 and 6), and three regions characterized by a constant rotation speed of the disc and the shaft (regions between

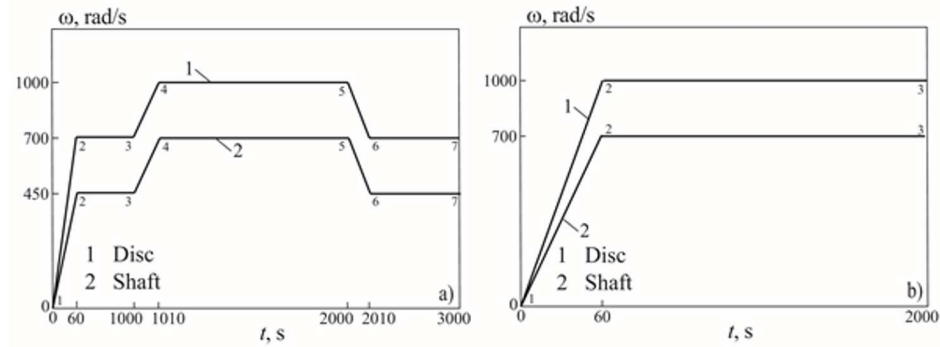


Figure 5: Cycle definition for thermal modelling (a) and coupled calculations (b).

ramp points 2 and 3, 4 and 5, 6 and 7).

For coupled thermal analysis, the rotor and the shaft, still at the initial time moment, accelerated to a velocity of 1000 rad/s and 700 rad/s in 60 s (region between ramp points 1 and 2) as shown in Fig. 5b. The total temperature in the inlet section of region I decreases from 500 K at time  $t = 0$  to 450 K at time  $t = 60$  s, and the total temperature in the inlet section of region II increases from 500 K at time  $t = 0$  to 700 K at time  $t = 60$  s. A long time interval ( $t_f = 2000$  s) is used to let the metal temperature reach a steady-state condition (region between ramp points 2 and 3). The use of a modified loading cycle in coupled calculations is due to the necessity of reducing the computational time.

### 4.3 Boundary conditions

At the initial time moment  $t = 0$  the metal has a uniform temperature distribution at 300 K. The formulation of the boundary conditions for the thermal simulation is explained in Fig. 2a. The thermal boundary conditions are identical in the 2D and 3D cases (in the 2D case the boundary conditions are applied to the edges and in the 3D one to faces). During simulation, boundary conditions on fluid/solid interface are defined by coupling procedure.

At boundaries 1, 2, and 3, the fluid convection at a known temperature of the wall derived from the loading cycle for a given time moment is taken into account. The heat transfer coefficient is calculated from empirical correlation for a free rotating disc derived in [25,26]. It is assumed that laminar flow conditions are realized at  $Re < 2.4 \times 10^5$ , and turbulent conditions are

realized at  $Re > 3 \times 10^5$ . In the interval between the limiting values, linear interpolation is used. The correlation parameter is the rotation speed of the disc.

In formulating the boundary conditions at boundaries 4 and 5, the formation mechanism of an adequate fluid flow in the rotating horizontal layer in the presence of a temperature gradient along the boundary is taken into account. The mass flow rate of the fluid in the annular gap between the disc and the shaft, the temperature and pressure are taken from the cycle definition. The heat transfer coefficient is calculated from the empirical correlation for the forced convection of the fluid in the annular gap, whose parameters are the cross-sectional area, hydraulic diameter and channel length.

At boundary 6, the heat transfer coefficient is found from empirical correlation for free convective fluid flow on a vertical plate. A correlation parameter is the plate length. As a wall temperature, the temperature obtained at boundary 10 is given.

The heat transfer coefficient at boundary 7 is calculated from empirical correlation for a free rotating disc [26] (as at boundaries 1–3). The boundary temperature is obtained as a result of mixing of the flows along boundaries 4 and 5, and boundary 6 (the heat balance condition is used).

To formulate the boundary conditions on the inner surface of a hole (boundaries 8 and 9) and calculate the heat transfer coefficient, the empirical correlation for the forced convection of fluid in the horizontal channel is used. Correlation parameters are the flow area, the hydraulic diameter, the channel length, and the mass flow rate of the fluid. The mass flow rate of the fluid (1/24 of the total rate of flow for the 2D model), the temperature and the pressure are derived from the loading cycle for a given time moment.

In formulation of boundary conditions at boundary 10, it is assumed that the fluid flowing past a given surface has a negligibly small heat capacity. The heat transfer coefficient is calculated from empirical correlation for free convection of the fluid in a horizontal cylinder. A correlation parameter is the Grashoff number calculated with characteristic diameter and rotation speed.

In the coupled thermal analysis, on the inner and outer surfaces of the rotor, on the surface of the shaft, as well as on the left and right surfaces of the disc (boundaries 1, 4–9), coupled boundary conditions are specified. The boundary conditions remain unaltered on the other walls of the model.

For the velocity on the shaft and disc surfaces (in regions I and II), no-slip and no-penetration boundary conditions are specified, as shown in Fig. 2. At the inflow boundaries, the mass flow rate ( $m = 0.63$  kg/s for region I and  $m = 2.25$  kg/s for region II) and the total temperature ( $T = 500$  K for region I and  $T = 700$  K for region II) are specified, and a static pressure ( $p = 5 \times 10^5$  Pa for region I and  $p = 10^6$  Pa for region II) is fixed on the outlet boundaries. The flow direction is assumed to be normal to the inlet boundary. The turbulent kinetic energy and its dissipation rate are specified on the inlet boundaries ( $k = 10^{-3}$  m<sup>2</sup>/s<sup>2</sup> and  $\varepsilon = 10^{-2}$  m<sup>2</sup>/s<sup>3</sup>). In the circumferential direction, periodic boundary conditions are used. To transfer data from the 3D CFD model to the 2D FEA model, averaging of the flow parameters in the circumferential direction is performed.

Wall functions are used to specify the turbulent kinetic energy and its dissipation rate near solid walls. The standard wall functions implementation in the CFD code sets the velocity at nodes on the wall to the velocity of the wall. The required walls shear stress from the log-law is achieved by modifying the turbulent viscosity on edges which are connected to the wall. This utilizes the assumption that the wall shear stress is uniform over the cell adjacent to the wall.

The linear and rotational Reynolds numbers calculated with the parameters in the inlet boundary and the rotation speed of the disc are  $8.89 \times 10^5$  and  $1.51 \times 10^4$  for region I, and  $4.12 \times 10^4$  and  $5.98 \times 10^4$  for region II, which corresponds to turbulent flow conditions.

#### 4.4 Mesh

The FEA mesh contains 2170 elements and 4804 nodes. The structured CFD mesh, used in region I and presented in Fig. 6a, contains 12768 cells and 14,820 nodes (the inner surface of the rotor and the shaft surface hold 741 faces each, the inflow and outflow boundaries contain 228 faces each). The structured CFD mesh, used in region II and shown in Fig. 6b, contains 30 3471 cells and 32 0512 nodes (1862 faces on the outer surface of the rotor, the left and right surfaces of the disc contain 3162 faces each, and the inflow and outflow boundaries contain 3591 faces each).

On all the surfaces that are of interest for coupled thermal analysis (the inner and outer surfaces of the rotor and the shaft surface) the near-wall coordinate  $y^+$  varies over a range acceptable for the application of the wall functions ( $35 < y^+ < 175$ ). On the left and right surfaces of the disc, the coordinate  $y^+$  has uniform distribution ( $y^+ \sim 120$ ).

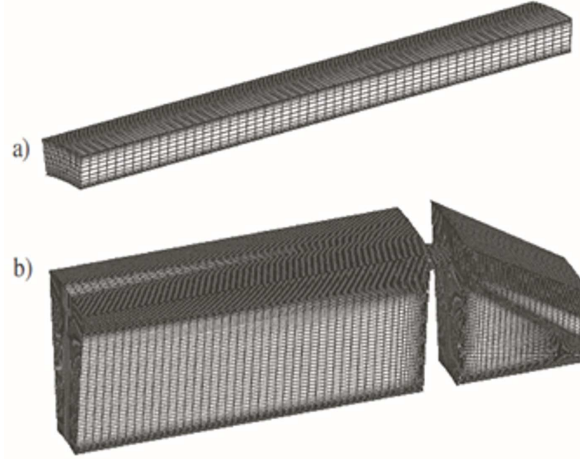


Figure 6: Structured meshes in domain I (a) and domain II (b).

A typical approach to determine the mesh independent solution for a given scenario is to perform the simulation with progressively smaller mesh cells, and then apply the Richardson extrapolation method. Mesh sensitivity tests are run in order to obtain a mesh independent solution. The results computed show that a mesh independent solution is obtained with the given mesh, therefore a further refinement of the mesh would not lead to significant improvements for this type of analysis.

#### 4.5 Coupling procedure

A maximum number of iterations for each CFD model is 100. This number of CFD iterations are performed per CFD analysis if no other convergence criteria are satisfied within the CFD model. The convergence condition is controlled by the temperature difference at the interface which equals 1 K.

It has long been recognized that there are situations where fluid properties are essentially independent of temperature, and the flow energy equation has no influence on the flow field. Selection of the energy equation only option assumes that the flow regime does not alter significantly from the original converged model.

#### 4.6 Stand-alone calculations

The temperature distributions along the outer surface of the shaft (line 1), and on the inner and outer surfaces of the disc (line 2 and line 3) are shown in Fig. 7, where  $l$  is the distance along the wall calculated from the left boundary. The kink of the line corresponds to a nodal point of the model. The temperature on the disc surface increases by about 100 K with increasing radial coordinate.

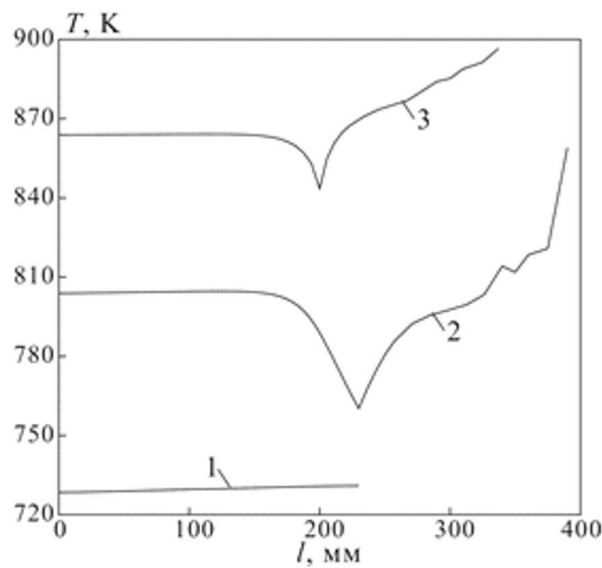


Figure 7: Temperature distributions on disc and shaft at time  $t = 2000$  s.

The time histories of the metal temperatures are shown in Figs. 8 and 9 (the results of calculations at points s1–s3, d1 and d2, d8 and d9, b3 and b4 are very similar and, therefore, are not shown in the figures). There is a good agreement between the results obtained in 2D and 3D formulations of the problem. The maximum difference between the metal temperatures at control points does not exceed 2 K (lines 3 and 4 in Fig. 9).

The flow in a hole is symmetric. Weak asymmetry of the flow takes place only in the upper and lower regions. In the lower part of the cavity located behind the hole, a recirculation zone occupying the entire volume of the computational domain is formed, as presented in Fig. 10. The secondary vortex is visible in the upper part of the domain.

Except for the small initial portion that is due to the influence of the

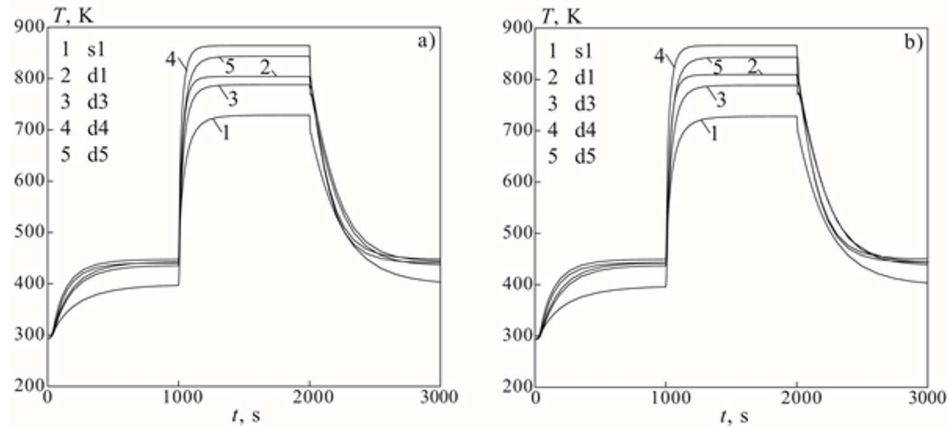


Figure 8: Time histories of metal temperatures at control points in 2D case (a) and 3D case (b) for non-coupled analysis.

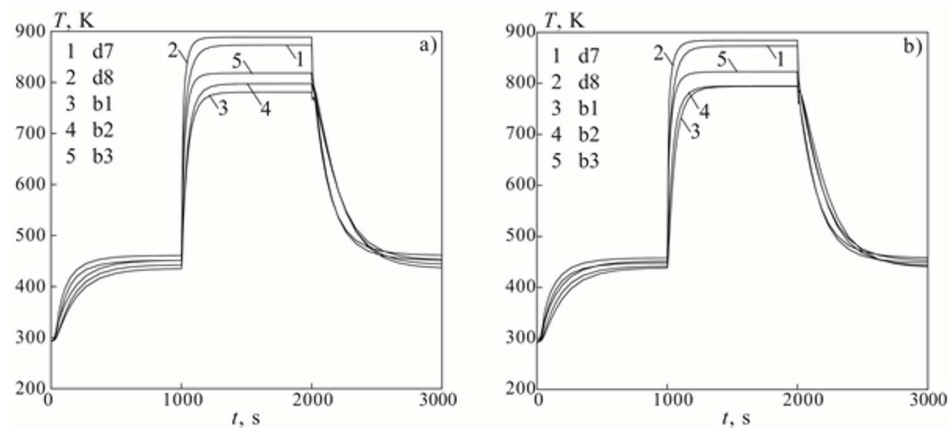


Figure 9: Time histories of metal temperatures at control points in 2D case (a) and 3D case (b) for non-coupled analysis.

flow conditions at the inlet boundary of the computational domain, the temperature distribution is uniform over the cross-section. This permits using the 2D model for simulation of coupled heat transfer in domain I.

The time histories of the metal temperatures at control points obtained with the 2D and 3D coupled thermal analysis are given in Figs. 11 and 12 (the results of calculations at point s1–s3, d1 and d2, d4 and d5, d8 and d9, b3 and b4 coincide and, therefore, are not presented). There is fairly good agreement between the calculations in the 2D and 3D calculations.

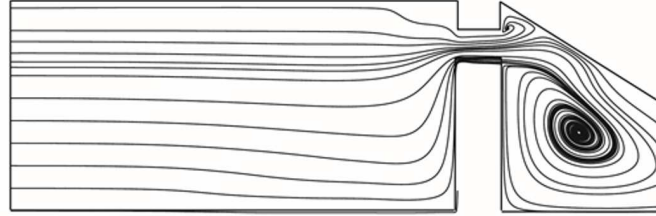


Figure 10: Streamlines in the meridional section of region II.

The largest discrepancy between the calculation results are observed at points b1 and b2 (see Fig. 12). The results of simulation, presented in Fig. 11 and 12, agree with the data obtained for the complete loading cycle. These results are shown in Figs. 8 and 9 for a time interval from 1000 s to 2000 s. The temperature calculation error corresponding to the steady-state conditions (horizontal region of the loading cycle) does not exceed 1 K.

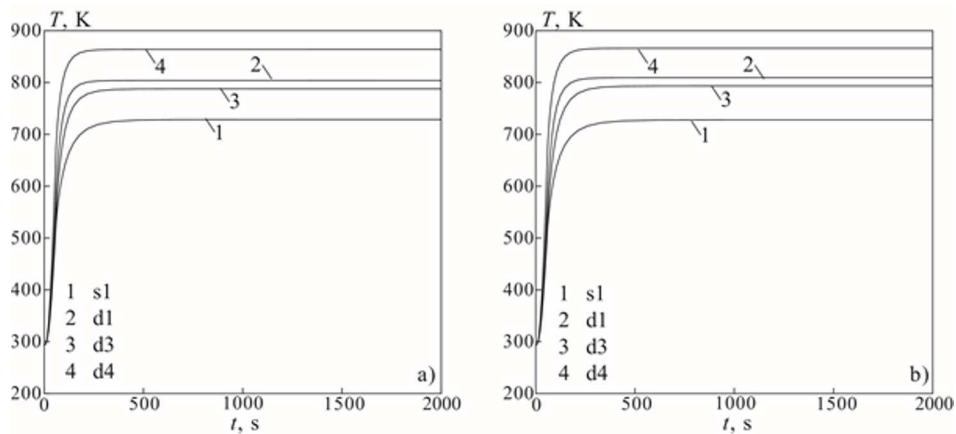


Figure 11: Time histories of metal temperatures at control points in 2D case (a) and 3D case (b) for coupled analysis.

## 5 Discussion

For the initial temperature field, the distribution obtained for the case of adiabatic walls is used. The temperature distributions along the outer surface of the shaft, and the inner and outer surfaces of the disc obtained

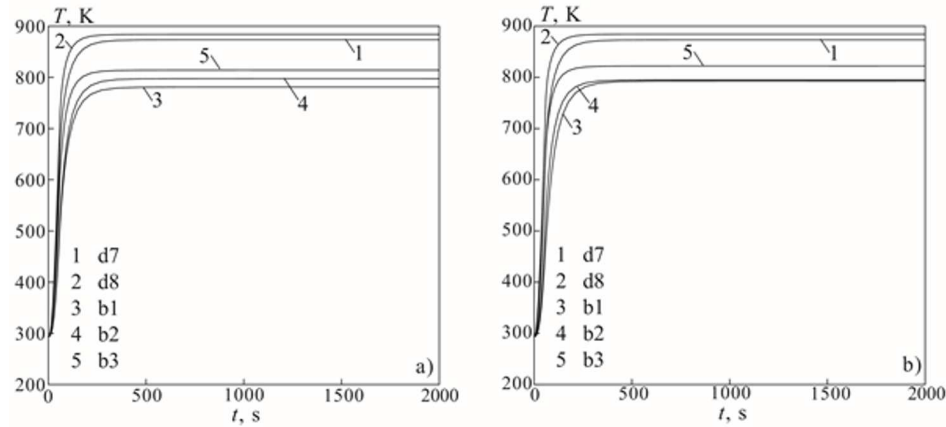


Figure 12: Time histories of metal temperatures at control points in 2D case (a) and 3D case (b) for coupled analysis.

in the coupled formulation agree fairly well with the data presented in Fig. 7 obtained with thermal boundary conditions based on the empirical correlations for the heat transfer coefficient. However, the increase in the disc surface temperature given by the coupled thermal analysis is somewhat smaller and equals 90 K.

Speed-up of computational procedure and number of time steps are presented in Tab. 1 for different number of iterations for computation of temperature field on every time step. The results are obtained for multigrid and GMRES solvers applied to solve energy conservation equation in the fluid domain (frozen flowfield).

Using GMRES method for solution of temperature equation and decreasing number of iterations per time step from 50 to 1, the metal temperature in control points changes less than 0.5 K.

## 6 Conclusion

An efficient FEA/CFD thermal coupling technique has been developed and demonstrated. The thermal coupling is realized through an iterative procedure between FEA and CFD calculations. The FEA simulation is treated as transient and the CFD calculations are regarded as steady. Communication between FEA and CFD calculations ensures continuity of temperature and heat flux.

Table 1: Speed-up of coupling procedure.

No.	Method of solution	Number of iterations	Speed-up	Number of time steps	
				1	2
1	Multigrid	10	3.23	30	26
2	Multigrid	25	1.78	22	24
3	Multigrid	50	1.56	18	21
4	GMRES	1	6.26	25	24
5	GMRES	2	3.15	28	25
6	GMRES	5	1.91	17	22
7	GMRES	10	1.18	15	23

To speed up the thermal coupling, steady CFD calculations are employed, considering that fluid flow timescales are much shorter than those for the solid heat conduction and therefore the influence of unsteadiness in fluid regions is negligible. To facilitate the thermal coupling, the procedure is designed to allow a set of CFD models to be defined at key time points/intervals in the transient cycle and to be invoked during the coupling process at specified time points. To further enhance computational efficiency, a frozen flow or energy equation only coupling option was also developed, where only the energy equation is solved while the flow is frozen in CFD simulation during the thermal coupling process for specified time intervals. Comparison of different methods, Multigrid and GMRES, shows that GMRES solver is more efficient in terms of number of computational step allowing to save computational time.

The results obtained are useful for design and optimisation of gas turbines and rotating disc cavity systems allowing an accurate prediction of fluid and metal temperatures.

**Acknowledgement** This work was financially supported by the Ministry of Education and Science of Russian Federation (agreement No 14.578.21.0203, unique identifier of applied scientific research RFMEFI57816X0203).

*Received 16 April 2018*

## References

- [1] PARESCHI G., FRAPOLLI N., CHIKATAMARLA S.S., KARLIN I.V.: *Conjugate heat transfer with the entropic lattice Boltzmann method*. Phys. Rev. E, **94**(2016), 013305.
- [2] ORLANDI P., SASSUN D., LEONARDI S.: *DNS of conjugate heat transfer in presence of rough surfaces*. Int. J. Heat Mass Tran. **100**(2016), 250–266.
- [3] DANG D.-D., PHAM X.-T., LABBE P., TORRIANO F., MORISSETTE J.-F., HUDON C.: *CFD analysis of turbulent convective heat transfer in a hydro-generator rotor-stator system*. Appl. Therm. Eng. **130**(2018), 17–28.
- [4] HWANG S., SON C, SEO D., RHEE D.-H., CHA B.: *Comparative study on steady and unsteady conjugate heat transfer analysis of a high pressure turbine blade*. Appl. Therm. Eng. **99**(2016), 765–775.
- [5] OKITA Y., YAMAWAKI S.: *Conjugate heat transfer analysis of turbin erotor–stator systems*. ASME Paper, 2002, GT2002-30615.
- [6] BOHN D., REN J., KUSTERER K.: *Conjugate heat transfer analysis for film cooling configurations with different hole geometries*. ASME Paper, 2003, GT2003-38369.
- [7] KUSTERER K., BOHN D., SUGIMOTO T., TANAKA R.: *Conjugate calculations for a film-cooled blade under different operating conditions*. ASME Paper, 2004, GT2004-53719.
- [8] LEWIS L.V., PROVINS J.I.: *A non-coupled CFD–FE procedure to evaluate windage and heat transfer in rotor–stator cavities*. ASME Paper, 2004, GT2004-53246.
- [9] SAUNDERS K., ALIZADEH S., LEWIS L.V., PROVINS J.: *The use of CFD to generate heat transfer boundary conditions for a rotor–stator cavity in a compressor drum thermal model*. ASME Paper, 2007, GT2007-28333.
- [10] REYHANI M.R., ALIZADEH M., FATHI A., KHALEDI H.: *Turbine blade temperature calculation and life estimation – a sensitivity analysis*. Propulsion and Power Research **2**(2013), 2, 148–161.
- [11] LI H., KASSAB A.J.: *A Coupled FVM/BEM approach to conjugate heat transfer in turbine blades*. ASME Paper, 1994, GT1994-1981.
- [12] LOUDA P., SVACEK P., FORT J., HALAMA J., KOZEL K: *Numerical simulation of turbine cascade flow with blade-fluid heat exchange*. Appl. Math. Comput. **219**(2013), 13, 7206–7214.
- [13] ILLINGWORTH J., HILLS N., BARNES C.: *3D fluid–solid heat transfer coupling of an aero-engine preswirl system*. ASME Paper, 2005, GT2005-68939.
- [14] MIRZAMOGHADAM A.V., XIAO Z.: *Flow and heat transfer in an industrial rotor-stator rim sealing cavity*. J. Eng. Gas Turb. Power **124**(2002), 1, 125–132.
- [15] VERDICCHIO J.A., CHEW J.W., HILLS N.J.: *Coupled fluid/solid heat transfer computation for turbine discs*. ASME Paper, 2001, GT2001-0123.
- [16] MOORE T.J., JONES M.R.: *Solving nonlinear heat transfer problems using variation of parameters*. Int. J. Therm. Sci. **93**(2015), 29–35.
- [17] LAUNDER B.E., SPALDING D.B.: *The numerical computation of turbulent flows*. Comput. Methods Appl. M. **3**(1974), 2, 269–289.

- 
- [18] KATO M., LAUNDER B.E.: *The modelling of turbulent flow around stationary and vibrating square cylinders*. Proc. 9th Symp. Turbulent Shear Flows, 16–18 Aug. 1993, Kyoto, 10.4.1–10.4.6.
- [19] CHEN W.L., LIEN F.S., LESCHZINER M.A.: *Computational modelling of turbulent flow in turbomachine passage with low-Re two-equation models*. Computational Fluid Dynamics. John Wiley & Sons, Chichester 1994, 517–524.
- [20] LESCHZINER M.A., RODI W.: *Calculation of annular and twin parallel jets using various discretization schemes and turbulent-model variations*. J. Fluid Eng. **103**(1981), 353–360.
- [21] ISAEV S.A., BARANOV P.A., USACHOV A.E., ZHUKOVA YU., VYSOTSKAYA A.A., MALYSHKIN D.A.: *Simulation of the turbulent air flow over a circular cavity with a variable opening angle in an u-shaped channel*. J. Eng. Phys. Thermophys. **88**(2015), 4, 902–917.
- [22] ISAEV S., BARANOV P., POPOV I., SUDAKOV A., USACHOV A., GUVERNYUK S., SINYAVIN A., CHYLUNIN A., MAZO A., KALININ E.: *Ensuring safe descend of reusable rocket stages – Numerical simulation and experiments on subsonic turbulent air flow around a semi-circular cylinder at zero angle of attack and moderate Reynolds number*. Acta Astronaut. 2017, 10.1016/j.actaastro.2017.10.028.
- [23] LARSON M.G., BENGZON F.: *The finite element method: theory, implementation, and applications*. Springer, 2013.
- [24] VOLKOV K.: *Multigrid and preconditioning techniques in CFD applications*. In: CFD Techniques and Thermo-Mechanical Applications (Z. Driss, B. Necib, H.-C. Zhang, Eds.), Springer Int. Publ., 2018, 83–149.
- [25] DORFMAN L.A.: *Hydrodynamic resistance and heat loss of rotating solids*. Edinburgh: Oliver & Boyd, 1963.
- [26] NORTHROP A., OWEN J.M.: *Heat transfer measurements in rotating disc systems – the free disc*. Int. J. Heat Fluid Fl. **9**(1988), 1, 19–26.